

REPORT DOCUMENTATION PAGE				Form Approved OMB No. 0704-0188	
Public reporting burden for this collection of information is estimated to average 1 hour per response, including the time for reviewing instructions, searching existing data sources, gathering and maintaining the data needed, and completing and reviewing this collection of information. Send comments regarding this burden estimate or any other aspect of this collection of information, including suggestions for reducing this burden to Department of Defense, Washington Headquarters Services, Directorate for Information Operations and Reports (0704-0188), 1215 Jefferson Davis Highway, Suite 1204, Arlington, VA 22202-4302. Respondents should be aware that notwithstanding any other provision of law, no person shall be subject to any penalty for failing to comply with a collection of information if it does not display a currently valid OMB control number. <b>PLEASE DO NOT RETURN YOUR FORM TO THE ABOVE ADDRESS.</b>					
1. REPORT DATE (DD-MM-YYYY) 25-06-2008		2. REPORT TYPE Technical Paper		3. DATES COVERED (From - To)	
4. TITLE AND SUBTITLE  <b>Results on Subcritical One-Phase Coaxial Jet Spread Angles and Subcritical to Supercritical Acoustically Forced Coaxial Jet Dark Core Lengths (Preprint)</b>				5a. CONTRACT NUMBER	
				5b. GRANT NUMBER	
				5c. PROGRAM ELEMENT NUMBER	
6. AUTHOR(S) Juan Rodriguez, Ivett A. Leyva, & Douglas Talley (AFRL/RZSA); Bruce Chehroudi (ERC)				5d. PROJECT NUMBER	
				5e. TASK NUMBER 23080533	
				5f. WORK UNIT NUMBER	
7. PERFORMING ORGANIZATION NAME(S) AND ADDRESS(ES)  Air Force Research Laboratory (AFMC) AFRL/RZSA 10 E. Saturn Blvd. Edwards AFB CA 93524-7680				8. PERFORMING ORGANIZATION REPORT NUMBER  AFRL-RZ-ED-TP-2008-260	
9. SPONSORING / MONITORING AGENCY NAME(S) AND ADDRESS(ES)  Air Force Research Laboratory (AFMC) AFRL/RZS 5 Pollux Drive Edwards AFB CA 93524-7048				10. SPONSOR/MONITOR'S ACRONYM(S)	
				11. SPONSOR/MONITOR'S NUMBER(S) AFRL-RZ-ED-TP-2008-260	
12. DISTRIBUTION / AVAILABILITY STATEMENT  Approved for public release; distribution unlimited (PA #08263A).					
13. SUPPLEMENTARY NOTES For presentation at the 44 <sup>th</sup> AIAA Joint Propulsion Conference, Hartford, CT, 20-23 July 2008.					
14. ABSTRACT  An investigation of the behavior of N2 gas-gas shear coaxial jet spread angles in conjunction with a comprehensive N2 shear coaxial jet dark core length analysis is presented. For the one-phase coaxial jet spread angle study, a total of 6 cases, corresponding to different momentum flux ratios (MR <sup>+</sup> ) at subcritical pressures are analyzed and compared to existing data. The measurements were extracted from 20 backlit images with the chamber to outer jet density ratio varying from 0.17-4.8. The objective of the second part of this work is to study the effect on the magnitude of the inner jet dark core length of transverse acoustic forcing at subcritical to supercritical pressure environments. The dark core length data comprises MR <sup>+</sup> from 0.02 to 23 with corresponding velocity ratios from 0.25 to 23. In these acoustically-forced cases, the resonant frequency of the system varied from 2.93 to 3.09 kHz and the maximum root-mean-square pressure variation with respect to total pressure was 4%. When comparing cases with very similar MR <sup>+</sup> , it was found that the relative acoustic excitation intensities for subcritical pressures were up to eight times stronger than near and supercritical chamber pressures. Despite that fact, the corresponding relative change in length of the dark core did not vary more than 50% between the three pressure regimes.					
15. SUBJECT TERMS					
16. SECURITY CLASSIFICATION OF:			17. LIMITATION OF ABSTRACT	18. NUMBER OF PAGES	19a. NAME OF RESPONSIBLE PERSON
a. REPORT	b. ABSTRACT	c. THIS PAGE			Dr. Douglas Talley
Unclassified	Unclassified	Unclassified	SAR	13	19b. TELEPHONE NUMBER (include area code) N/A

# RESULTS ON SUBCRITICAL ONE-PHASE COAXIAL JET SPREAD ANGLES AND SUBCRITICAL TO SUPERCRITICAL ACOUSTICALLY FORCED COAXIAL JET DARK CORE LENGTHS (PREPRINT)

Juan I Rodriguez<sup>°</sup>, Ivett A Leyva<sup>\*</sup>, Bruce Chehroudi<sup>+</sup>, Douglas Talley<sup>\*</sup>

<sup>°</sup>Graduate Student, UCLA, Los Angeles, CA

<sup>\*</sup>AFRL/RZSA, Edwards AFB, CA

<sup>+</sup>ERC Inc., Edwards AFB, CA

An investigation of the behavior of N<sub>2</sub> gas-gas shear coaxial jet spread angles in conjunction with a comprehensive N<sub>2</sub> shear coaxial jet dark core length analysis is presented. For the one-phase coaxial jet spread angle study, a total of 6 cases, corresponding to different momentum flux ratios (MR's) at subcritical pressures are analyzed and compared to existing data. The measurements were extracted from 20 backlit images with the chamber to outer jet density ratio varying from 0.17-4.8. The objective of the second part of this work is to study the effect on the magnitude of the inner jet dark core length of transverse acoustic forcing at subcritical to supercritical pressure environments. The dark core length data comprises MR's from 0.02 to 23 with corresponding velocity ratios from 0.25 to 23. In these acoustically-forced cases, the resonant frequency of the system varied from 2.93 to 3.09 kHz and the maximum root-mean-square pressure variation with respect to total pressure was 4%. When comparing cases with very similar MR's, it was found that the relative acoustic excitation intensities for subcritical pressures were up to eight times stronger than near and supercritical chamber pressures. Despite that fact, the corresponding relative change in length of the dark core did not vary more than 50% between the three pressure regimes.

## INTRODUCTION

One of the mechanisms responsible for inducing combustion instabilities in Liquid Rocket Engines (LRE's) is the interaction of the injector flow with the combustion chamber acoustic modes. Given the widespread use of coaxial injectors in LRE's, such as those used for the J-2 engine and the Space Shuttle Main Engine, understanding the phenomena that could lead to unstable behavior in these propulsion systems is of primary importance. Recent improvements experienced in LRE performance have increased mean combustion chamber pressures over the critical value of some propellants. Therefore, one of the objectives of this work is to perform experiments in the supercritical pressure regime.

Also of interest in LRE studies is the momentum flux ratio (MR) and velocity ratio (VR) between the outer jet and the inner jet. It has been found that combustion is more stable at high velocity ratios [1]. Marshall et al. [2] performed experiments at 1.53 MPa with maximum amplitudes of 4% of the peak-to-peak pressure perturbation ( $\Delta p_{\text{peak-to-peak}}$ ) as a fraction of mean chamber pressure ( $p_{\text{mean}}$ ). They studied the influence of mass flow rate, mixture ratio, injector and nozzle positions and chamber pressure on the spontaneous excitation of the transverse modes of their three-dimensional rectangular chamber. They found that the first mode of the largest dimension of the chamber showed stronger response when the injector was positioned near a pressure antinode location. In another study, Richecoeur et al. [3] observed that combustion is more sensitive to acoustics at low outer jet velocities. They obtained strong coupling between the combustion products from three coaxial CH<sub>4</sub>/O<sub>2</sub> injectors and an imposed transverse acoustic field reaching 7%  $\Delta p/p$  with a mean chamber pressure of 0.9 MPa.

The first part of this work consists of an analysis of the outer jet angles of a gaseous coaxial jet flow exiting into a gaseous atmosphere. In a thorough experimental analysis, Chehroudi et al. [4] showed for the first time that the spreading angle growth rate of single round jets at supercritical pressure and temperature agreed quantitatively with theoretical predictions from previous investigations [5-7]. Chehroudi et al. also compiled experimental data from different researchers which spanned four orders of magnitude in the ratio of the chamber density to the jet density, which is an important parameter for single jets ejecting into a quiescent environment. For coaxial jets at subcritical, nearcritical and supercritical pressures and MR's varying from 0.4 to 30, Leyva et al. [8] found that the near-field outer jet spreading angle was about constant (11°). This data comprised gas-liquid, supercritical-liquid-like and supercritical-supercritical combinations of the outer and inner jet respectively. The data compared well with CFD

simulations completed for two conditions ran in this lab. However, the spreading angles were consistently lower than other experimental data (mostly gas-gas) and theoretical predictions for 2D jet spreading angles and shear layer growth. One of the motivations of this study is to complement this data set with gas-gas data and see if the spreading angles remain about constant.

In this study, a complete set of subcritical to supercritical measurements of the dark core length of a coaxial jet is also presented, building upon data reported previously by the authors [8,9]. A transverse acoustic field is set up using two acoustic drivers and the phase between them is varied so the coaxial jet can be exposed to different acoustic conditions. The chamber pressure,  $\Delta p/p$  and MR are considered to characterize the effects of this transverse acoustic field on the coaxial injector flow. The effect of the magnitude and phase of the pressure oscillations is characterized in this study by examining the behavior of the dark-core length of the inner jet. Leyva et al. [10,11] used a configuration where the position of the injector with respect to the acoustic field was fixed, since only one acoustic driver was used to generate the transverse acoustic field with a reflective wall placed at the other end of the test section. This study reported that for MR's between 1 and 4 the effects of acoustic forcing on the coaxial jet dark core length were the most significant. The findings of this early configuration were consistent with a later study with two acoustic sources by Leyva et al. [8] where maximum changes in dark core length for subcritical pressures were statistically significant for an MR of 2.6 but not for an MR of 1. The nearcritical and supercritical data reported in this study will be compared to the subcritical trends mentioned in these previous reports.

## EXPERIMENTAL SETUP

The Cryogenic Supercritical Laboratory (EC-4) at the Air Force Research Laboratory (AFRL) at Edwards Air Force Base, CA, was the facility used to conduct the experiments in this study. The main chamber and the supporting systems are shown in Figure 1. Ambient temperature  $N_2$  is used to supply the inner and outer jet and also for chamber pressurization. Heat exchangers (HE's) using liquid nitrogen obtained from a cryogenic tank were used to cool the inner and the outer jets. One heat exchanger was used for the inner jet and two others for the outer jet. For the outer jet flow, the option to bypass one of the HE's to modify the cooling pattern is available. In order to control the temperature of the jets, the mass flow rates of liquid nitrogen through the HE's are modified accordingly. To avoid difficulties with mass flow rate measurement at cryogenic temperatures, these rates are measured with Porter® mass flow meters (122 and 123-DKASVDAA) at ambient conditions. Both the inner and the outer jet flow through an injector assembly (see Fig. 2) which exits to an inner chamber built and housed inside the main chamber so that the amplitude of the acoustic oscillations are maximized at the test section. This inner chamber is 6.6 cm high, 7.6 cm wide and 1.3 cm deep (see Fig. 1).

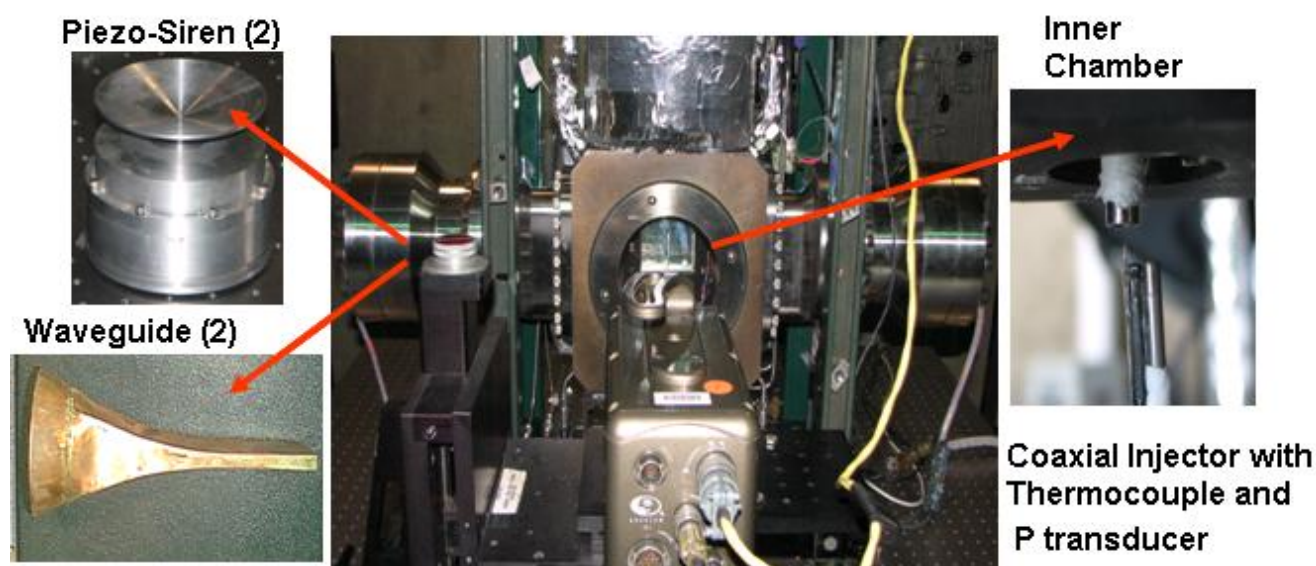


**Figure 1. Overview of the experimental apparatus**

The inner tube making the inner jet has an inner diameter,  $D1$ , of 0.51 mm with length-to-diameter ratio of 100. The inner jet exit plane is recessed by 0.25 mm from the outer jet. The outer annular jet's inner diameter,  $D2$ , is 1.59 mm with outer diameter,  $D3$ , of 2.42 mm. For the outer jet, the length-to-mean-width of the annular passage is 67. Detailed dimensions of the coaxial injector tip are shown in Fig. 2.

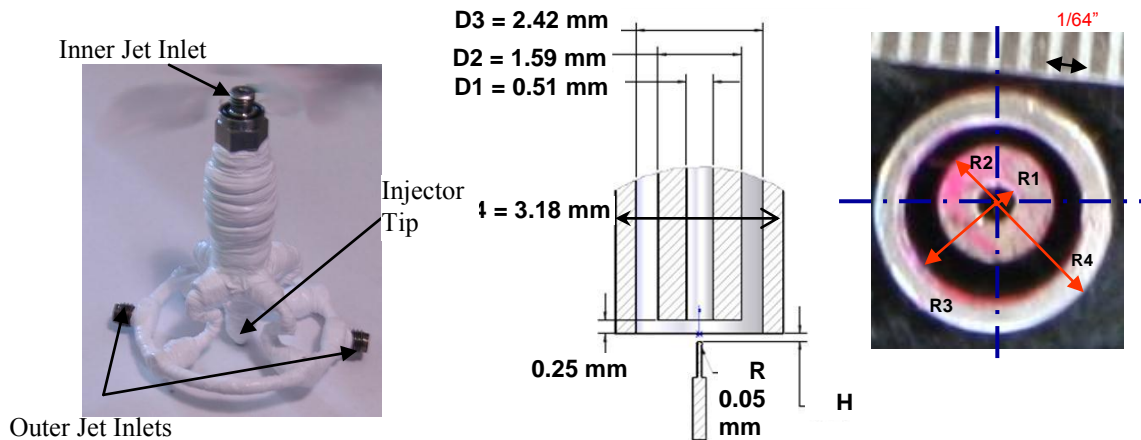


**Figure 2. Image and tip geometry of the shear coaxial injector used in this study.**

The temperature of the jets was measured using an unshielded type E thermocouple with a bead diameter of 0.1 mm. The accuracy of this thermocouple was checked with an RTD and found to be  $\pm 1$  K. The chamber pressure was measured with a Stellar 1500 transducer and a Kulite® XQC-062 pressure transducer was used to measure the pressure near the location of the thermocouple tip at a sampling frequency of 20 kHz (see right picture in Fig. 1). Two linear positioning stages built by Attocube Systems AG were used to move the pressure transducer and the thermocouple in the plane perpendicular to the jet axis. Each stage has a range of about 3 mm in 1 dimension with step sizes in the order of 0.01 mm. One stage was placed on top of the other with their axis of movement perpendicular to each other for a total maximum examination area of 3 mm by 3 mm. The thermocouple and pressure transducer were fixed to a custom made probe stand mounted on top of the positioning assembly. In turn, the linear stages were placed at the top end of a shaft that rested on a large 10-cm range linear stage built by SETCO™ outside the main chamber. Since the temperature probe approached the coaxial jet from the bottom and it had sufficient range, it was capable of getting arbitrarily close to the exit plane of the coaxial jet. In fact, the thermocouple was even been used to measure the temperature within the recess of the inner jet. Non-dimensional quantities such as  $Re$ ,  $We$ ,  $VR$  and  $MR$  for a given condition were calculated using the measured flow rates, the mean chamber pressure and jet temperatures in conjunction with NIST's REFPROP® database [12,13]. Density, viscosity, and surface tension values were obtained from these properties. For reference, the critical temperature of  $N_2$  is 126.2 K and its critical pressure is 3.39 MPa.

Flow visualization was achieved with a Phantom® 7.1 CMOS camera. The camera can be seen facing the main chamber in the center picture of Fig. 2. Backlit images with a resolution from 128x224 to 196x400 pixels were obtained, with each pixel representing an area of approximately 0.08 mm by 0.08 mm. The framing rate was 20-25 kHz. The number of images saved per run was 1000 on average. The jet was backlit using a Newport® variable power arc lamp set at 160 W. For the analysis of the one-phase subcritical coaxial jet data, the jet spread angle between the outer jet and the chamber was measured directly from 20 backlit images. The spreading angle for this study was defined to start from the point where the jet starts to grow (approximately 2 to 4  $D1$  downstream of the exit plane) to 10 $D1$ . Therefore this can be interpreted as an initial spread angle. Figure 3 shows a typical image and how the spreading angle is measured. Only  $\alpha_1$  and  $\alpha_4$  are visible and measured. The angles  $\alpha_2$  and  $\alpha_3$  are not visible in the backlit images. They are indicated to complete a conceptual picture of the spreading of the jet.

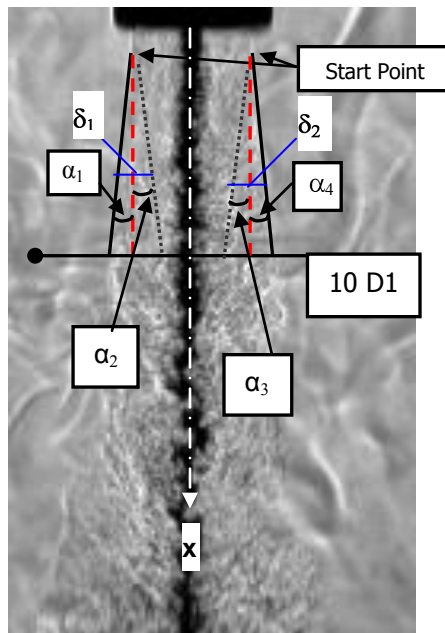


**Figure 3. Image showing how the spreading angle is measured.**

The dark core lengths were measured from 998 images using a MATLAB<sup>®</sup> subroutine based on the Otsu technique [14] to find a grayscale threshold which helps distinguish the inner core from the rest of the image (see Fig. 4). More details on how the dark core is defined and measured can be found in previous papers from this group [10,11]. Essentially, the colder inner jet in our experiments appears as a dark central feature on the images surrounded by a warmer outer jet. The axial dark core length,  $L_{\text{axial}}$ , is the projection of the inner jet before its first break along the axis parallel to the jet flow. The dark core length is a qualitative indicator of mixing. The shorter it is the faster mixing is occurring between the two jets. The dark core itself as a parameter does not have a unique definition. Different definitions and measuring techniques change its absolute magnitude. Thus, more value is placed on the trends and relative changes seen on the dark core as operating conditions change than on the actual absolute magnitudes.

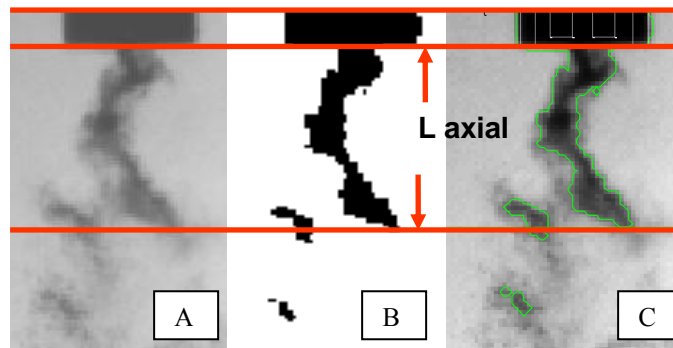


**Figure 4. Definition of axial dark core length,  $L_{\text{axial}}$ . [A] Typical image. [B] Original image after a threshold has been applied to a binary image. [C] Contour from which the axial length is calculated.**

The two piezo-sirens used to generate the transverse acoustic field were custom-designed by Hersh Acoustical Engineering, Inc. (see Fig. 1). In principle, a sinusoidal voltage signal moves the piezo element which has an

aluminum cone attached to it producing acoustics waves. When the two drivers have a zero degree phase angle difference they move in opposite directions. On the contrary, when the two drivers have a 180-degree phase difference the cones move in the same direction, ‘chasing’ each other. This behavior is represented by the sketches in Fig. 5. A Fluke® signal generator was used to drive the piezo-sirens with a sinusoidal wave at a chosen driving frequency and phase angle between them. The frequency was manually varied until the highest amplitudes of the pressure waves were obtained. These frequencies spanned a range between 2.93 and 3.09 kHz. Then the signals were amplified and fed to the piezo-sirens with the voltage supplied to each driver kept constant. A waveguide with a catenary contour was used to guide the waves from a circular cross-section at the end of the aluminum cone to the rectangular cross-section of the inner chamber.

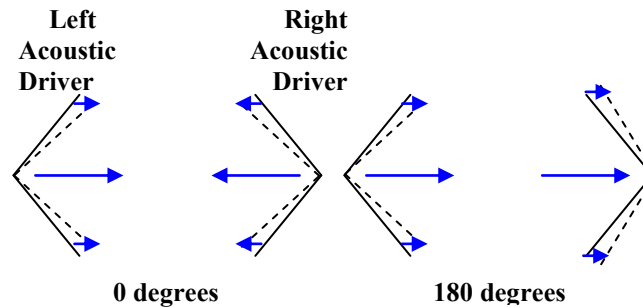


**Figure 5. Simplified diagram of the two acoustic drivers at a 0° and 180° phase angle.**

## RESULTS

### A. Subcritical One-Phase Outer Jet Spreading Angles.

One of the areas of interest in coaxial jet behavior is the situation where both fuel and oxidizer are injected into the combustion chamber in the gaseous phase. The purpose of this study is to complement previous work [8] where for subcritical pressures, the inner jet temperature was either a few degrees below or at the saturation temperature, and the outer jet was in the vapor phase, therefore having two-phase flow. For near and supercritical pressures, the inner and the outer jet were mostly both in the supercritical region, and therefore constituted one-phase flows but certainly not gas-gas flows. For a few cases, the inner jet was a few degrees below the critical temperature and therefore had a liquid-like-supercritical combination. Thus, the present work aims to complete this set of coaxial jet spreading angle measurements and make gas-gas data available since it is the most reported type of data in the literature for coaxial jets.

Angle measurements were processed from 6 MR's starting at 0.013 and up to 2.0. To generate these cases, the inner jet mass flow rate was fixed and the outer jet mass flow rate was varied. The temperatures were recorded to obtain the different thermodynamic variables used in the study. A visual inspection of at least 20 randomly-selected images for each case was performed. From each picture a left angle ( $\alpha_1$ ) and a right angle ( $\alpha_4$ ) were obtained. These angles were added and a total angle was found as shown in Figure 6. The plot shows an increasing angle as the momentum flux ratio goes up. This behavior is quite different to previous results reported by our group for different running conditions [8] where the outer jet spreading angle was about constant at 11°. In the plot shown, the trend starts with a very low momentum flux ratio (0.013) and a negative spreading angle (- 7°) which indicates that outer jet width is decreasing as it exits the tip of the injector. The next MR is 0.037 and in this case the coaxial jet shows an angle of 4°. The following MR's surveyed have angles (9-10°) which are similar to the constant angle (11°) obtained in the previous work mentioned above. Finally, the last MR of 2.0 has a total angle of 15°. This initial trend identifies conditions where the behavior of vapor-phase subcritical coaxial jets differs from the observed behavior of previous subcritical two-phase and near and supercritical experiments.

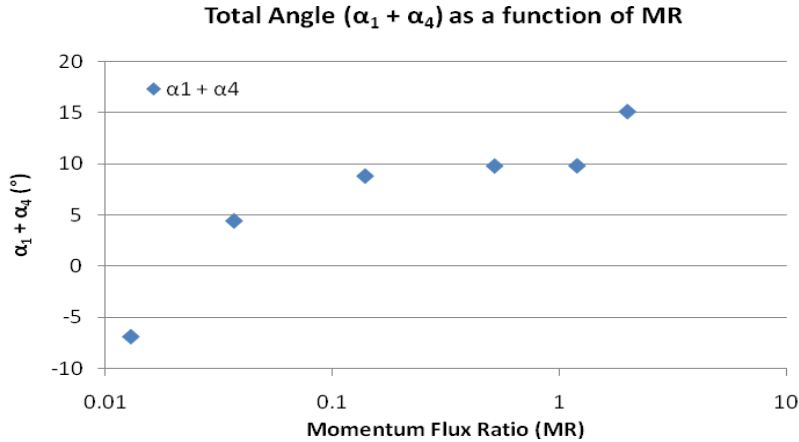


**Figure 6. Outer jet spread angle measurements for one-phase coaxial jet at subcritical pressures.**

To compare the results from these gas-gas experiments with other available data, a plot of the spreading angle growth rate as a function of the density of the chamber, the density of the outer jet and the momentum flux ratio is shown in Figure 7. The exact variable to which the spreading angle was compared is the ratio of the chamber density to that of the outer jet times the square root of the momentum flux ratio. The reason we incorporated MR to the more widely used chamber to outer jet density ratio is to bring in the effects of the inner jet on the outer jet spreading angle. A square root was used so that the outer jet density would not be cancelled and also because from previous studies [10,15] it was found this was an important scaling parameter for shear coaxial jets. For  $MR > 0.1$  cases it is interesting to notice that the new one-phase subcritical data (green triangles) clusters well with previous data from our group (blue triangles) and computational results using the same injector geometry that was used for this study (light green and dark orange squares). Data gathered from other researchers [5-7,16] and theoretical predictions show larger angles. One of the possible explanations for these larger angles as compared to the shorter angles obtained in our studies could be explained by the injector geometry used. The particular configuration used in our studies, which is the same geometry used by Liu et al. [17], produces a large recirculation zone between the inner jet and the outer jet at the inner jet exit location (see Fig. 2). This recirculation zone does not exist in coaxial jet geometries where the inner jet and the outer jet are separated by a very thin wall or for two-dimensional shear layer mixing studies where the flows mixing at two different velocities are assumed to have wall of negligible thickness between them. The exact mechanism responsible for the smaller outer jet spreading angles is still being understood.

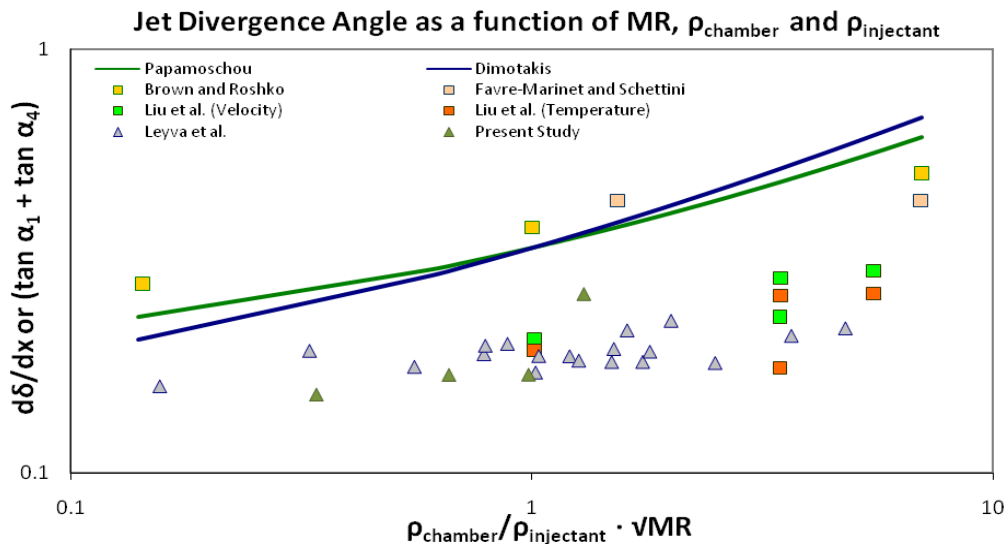


**Figure 7. Outer jet spread angle measurements compared to jet divergence angle theoretical predictions and other single jet and coaxial jet spreading angle experimental data.**

## B. Subcritical to Supercritical Dark Core Length Measurements.

For the second part of this paper, results on the dark core length of the inner jet of a coaxial jet flow at subcritical to supercritical chamber pressures where the flow was exposed to a transverse acoustic field will be presented. The results are drawn from a complete set of data where at least 6 cases are reported for each of the three mean chamber pressure conditions surveyed: subcritical, nearcritical and supercritical. The amplitude of the root-mean-square of the pressure perturbations compared to the mean chamber pressure ranged from 1 to 4 %, the VR varied from 0.25 to 23 and the MR from 0.02 to 23. A complementary analysis on this data will be presented by Leyva et al. [18]

Two acoustic sources were used to generate the transverse acoustic field inside the inner chamber of the experimental apparatus. To expose the coaxial jet flow to different acoustic conditions, the phase between the two acoustic sources was varied from  $0^\circ$  to  $360^\circ$  in steps of  $45^\circ$ . A measurement of the root-mean-square values of the pressure at each phase angle condition can be observed for a nearcritical case in Figure 8.

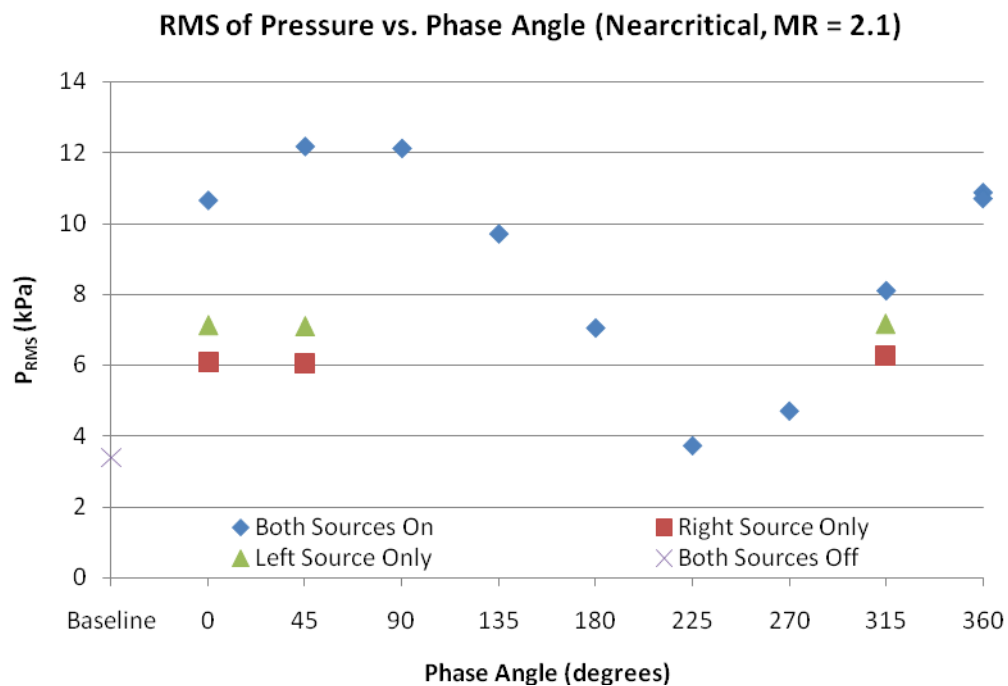


**Figure 8. RMS of chamber pressure versus phase angle between acoustic sources for the nearcritical case with MR = 2.1 (give id number for this case).**

To have a better understanding of the chamber environment during these tests, the time history of the chamber pressure during different transverse acoustic excitation conditions was plotted on the right column of Figure 9. Each plot on the left column of Figure 9 corresponds to the plot to the right. The image shows how the two acoustic sources combine to expose the jet to different pressure perturbation conditions at the coaxial jet center depending on the phase difference between them. Though ideally a maximum pressure perturbation should be achieved at  $0^\circ$  and the minimum at  $180^\circ$  such as in the supercritical case of Figure 9, maxima were observed as low as  $315^\circ$  ( $-45^\circ$ ) such as in the subcritical case for the same figure and as high as  $45^\circ$  such as in the nearcritical case. The search for an explanation for this phenomenon is still ongoing. Though not always at the same phase angles for all cases, the coaxial jet was exposed to different acoustics conditions ranging from minimum to maximum pressure and velocity perturbations. These oscillatory motions affected the jet behavior and the objective of this study was to quantify and understand the effects of these different acoustic conditions on the fluid mechanics of the jet.

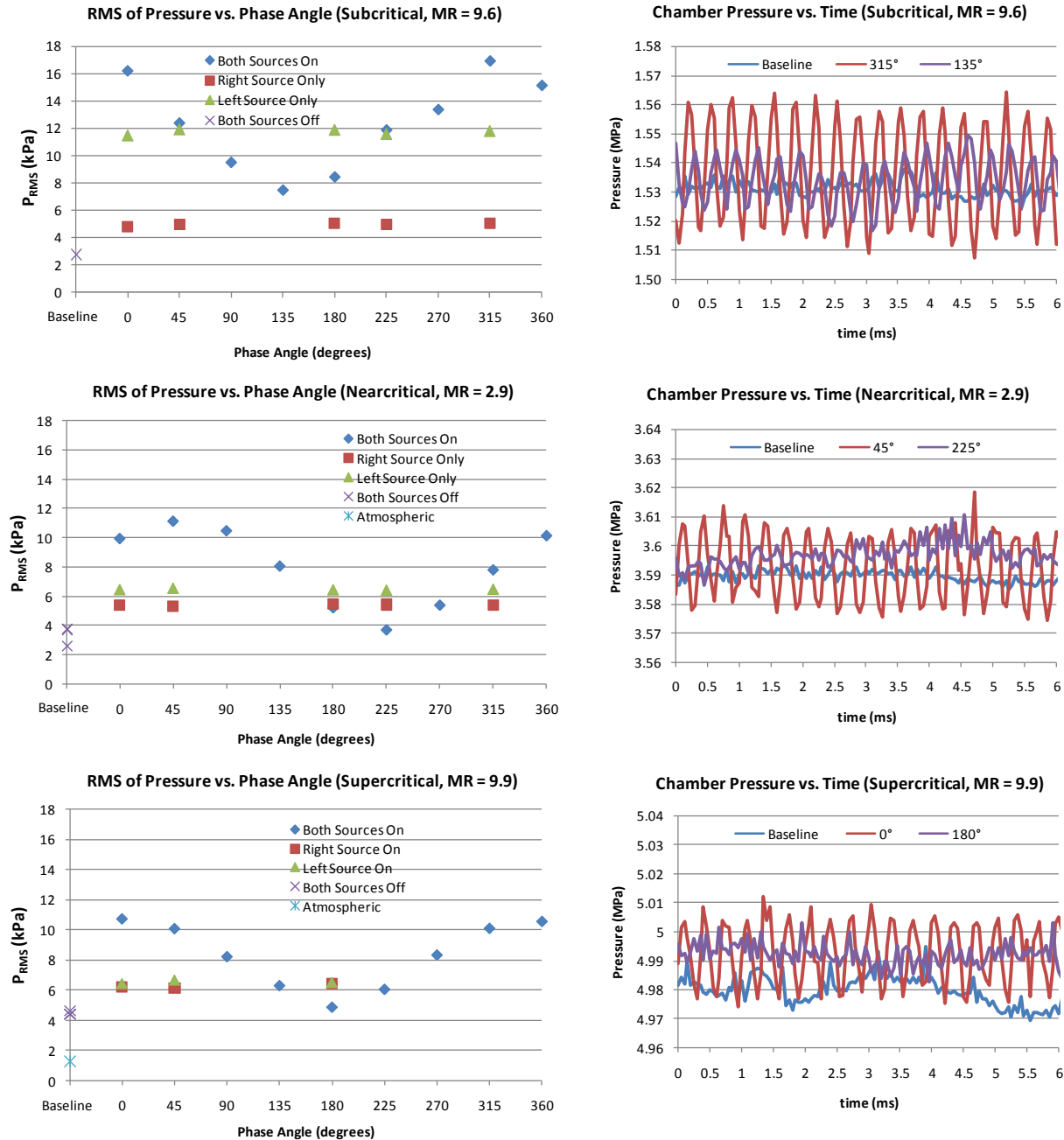


**Figure 9. RMS of chamber pressure vs. phase angle compared to chamber pressure as a function of time for one particular MR case at each of the three pressure conditions examined this study.**

The results of the dark core length change at different MR's and mean chamber pressure conditions are presented next. The ratio of the length of the dark core with acoustics to the length of the dark core with no acoustics ( $L_{acoustics}/L_{no\ acoustics}$ ) and the peak-to-peak pressure perturbation as a percentage of the mean chamber pressure ( $\Delta p_{peak-to-peak}/p_{mean}$ ) both as a function of the phase angle between acoustic sources are shown in Figure 10. In these series of plots, one of the most interesting observations is that for a given momentum flux ratio, the dark core length results from subcritical, nearcritical and supercritical tests do not show much difference among them at each phase angle condition. For instance, despite the relative acoustic excitation intensities varying as much as eight times from subcritical to supercritical chamber pressures, for an MR near 1.0, the change in normalized dark core length ( $\langle L_{acoustics}/L_{no\ acoustics} \rangle_{MAX} - \langle L_{acoustics}/L_{no\ acoustics} \rangle_{MIN}$ ) at any given phase angle was not more than 35% of the value of the minimum normalized dark core length at that phase angle ( $\langle L_{acoustics}/L_{no\ acoustics} \rangle_{MIN}$ ). In fact, still for an MR near

1.0, for most phase angles this change was not higher than 21% (see upper right corner plot in Fig. 10). Momentum flux ratios of 2.5 and 9.5 show similar trends in the change in normalized dark core length at any given phase angle with the largest change ( $\langle L_{\text{acoustics}}/L_{\text{no acoustics}} \rangle_{\text{MAX}} - \langle L_{\text{acoustics}}/L_{\text{no acoustics}} \rangle_{\text{MIN}}$ ) being not higher than 50% of the value of the minimum normalized dark core length ( $\langle L_{\text{acoustics}}/L_{\text{no acoustics}} \rangle_{\text{MIN}}$ ) at that phase angle as can be seen in the mid right and lower right corner plots in Fig. 10. Overall, these results show a very interesting trend which suggests that a normalized dark core length behavior which is independent of mean chamber pressure.

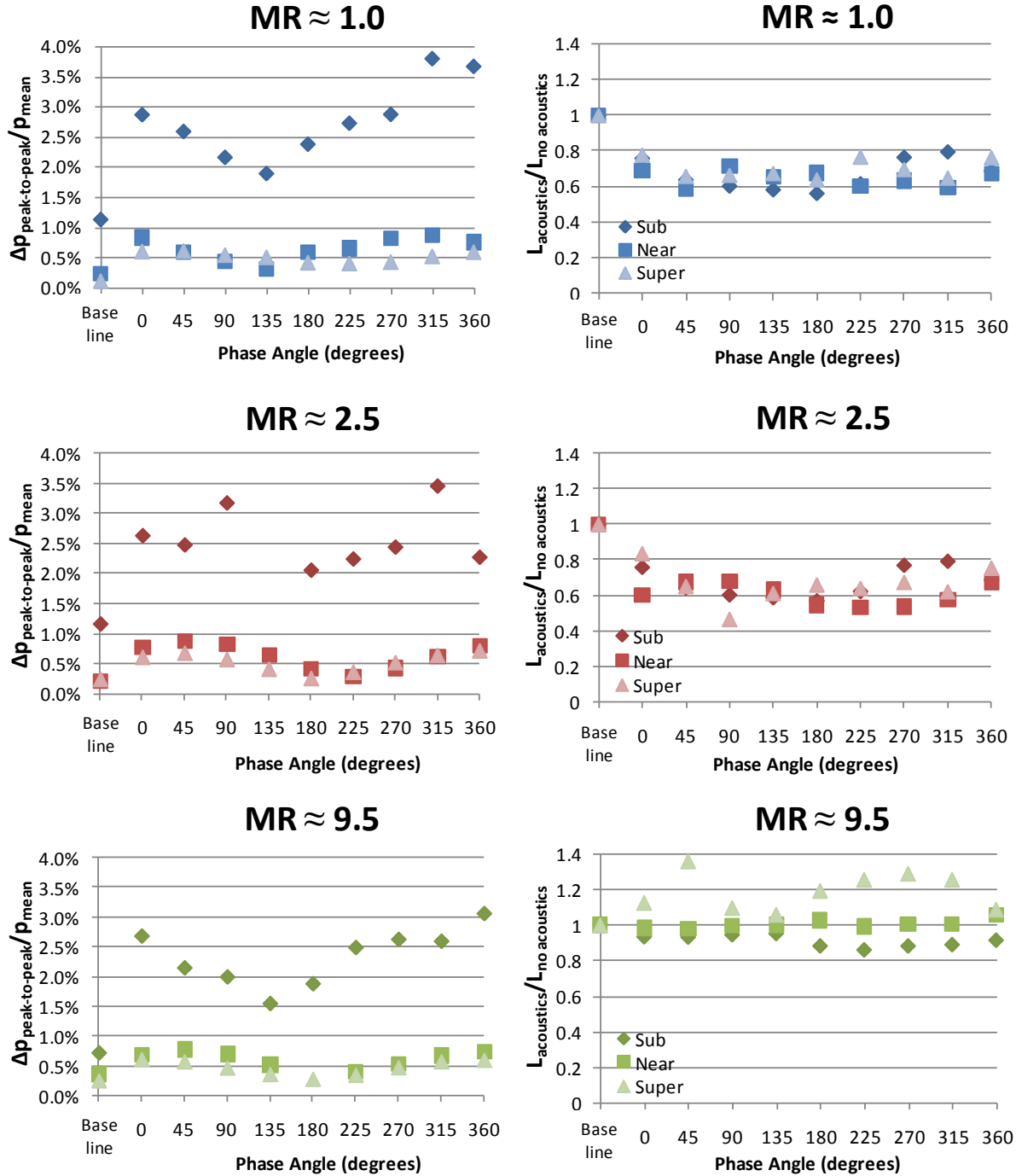
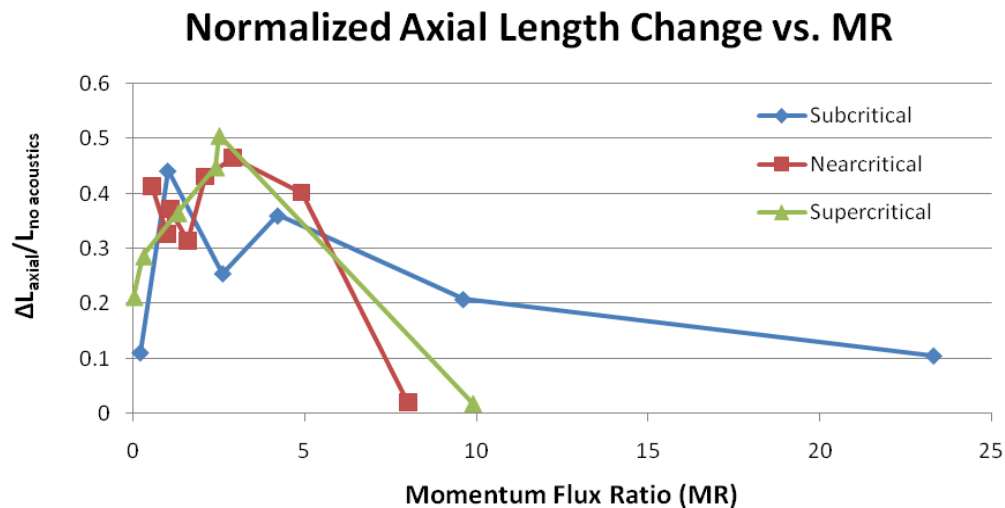


Figure 10. Peak-to-peak pressure perturbation ( $\Delta p_{\text{peak-to-peak}}$ ) as a percentage of the mean chamber pressure ( $p_{\text{mean}}$ ) and dark core length with acoustics ( $L_{\text{acoustics}}$ ) over dark core length without acoustics ( $L_{\text{no acoustics}}$ ) versus phase angle between acoustic sources for sub, near and supercritical pressures at MR  $\approx 1.0$ , 2.5 and 9.5.

A plot that compiles all the dark core length data is shown in Figure 11. To make this graph, the difference between the baseline length or the length of the dark core with no acoustics and the length of the dark core with acoustics ( $L_{\text{no acoustics}} - L_{\text{acoustics}}$ ) was found for each phase angle at a given mean chamber pressure and MR and the maximum was selected. This quantity was termed “axial length change” and then the normalized axial length change ( $\Delta L_{\text{axial}}/L_{\text{no acoustics}}$ ) was plotted versus MR for three mean chamber pressures. The overall trend for all pressure conditions shows that at very low MR's (< 0.5) the normalized axial length change drops below 30%. Next, the range of values of MR between 0.5 and 5 shows normalized axial length changes between 30 to 50%. The sole exception is the subcritical case with an MR of 2.6 which has a normalized axial length change of approximately 25%. All the cases with an MR greater than 5 show normalized axial length changes close to 20% or below. Though not in a very clear fashion, this plot confirms earlier statements by our group [8,9] suggesting a range of MR's in which the acoustic forcing has more influence on injector flow mechanics as suggested by its impact on the axial dark core length of the jet.



**Figure 11. Maximum length change between dark core length without acoustics and dark core length with acoustics ( $\Delta L_{\text{axial}}$ ) divided by the dark core length without acoustics ( $L_{\text{no acoustics}}$ ) for each MR case.**

## CONCLUSIONS

This study complemented previous work done at AFRL on shear coaxial jet spreading angles and dark core length measurements from subcritical to supercritical pressures. From the gas-gas coaxial jet experiments, it was found that the outer jet spreading angle increased with MR, in contrast with previous results showing essentially a constant angle for liquid-gas subcritical conditions, and a wide variety of supercritical conditions. In regard to the dark core length analysis for a given momentum flux ratio, the dark core length results from subcritical, nearcritical and supercritical tests did not show much difference among them at each phase angle condition. For instance, despite the relative acoustic excitation intensities varying as much as eight times from subcritical to supercritical chamber pressures, for an MR near 1.0, 2.5, and 9 the change in normalized dark core length at any given phase angle was not more than 50% of the value of the minimum normalized dark core length at that phase angle. In fact, for MR near 1.0, for most phase angles this change was not higher than 21%

## ACKNOWLEDGEMENTS

The authors would like to thank Lt. Jeff Graham for his valuable help processing the gas-gas coaxial jet angle data, and his assistance with the development of the visualization technique and the installation of the data acquisition system. They also express their appreciation to Mr. Randy Harvey for his invaluable contributions in running and maintaining the facility. This work is sponsored by AFOSR under Mitat Birkan, program manager.

## REFERENCES

1. Hulka, J., Hutt, J. J., *Liquid Rocket Engine Combustion Instability*, AIAA Progress in Astronautics and Aeronautics, Yang, V., Anderson W. E., Eds., 1995, p. 40.
2. Marshall, W., Pal, S., Woodward, R., Santoro, R. J., Smith, R., Xia, G., Sankaran, V., Merkle, C. L., "Experimental and Computational Investigation of Combustor Acoustics and Instabilities, Part II: Transverse Modes," *AIAA-2006-0538*
3. Richecoeur, F., Scouflaire, P., Ducruix, S., Candel, S., *Journal of Propulsion and Power* 4:790-799 (2006).
4. Chehrودي, B., Talley, D., Coy, E., "Visual characteristics and initial growth rates of round cryogenic jets at subcritical and supercritical pressure", *Physics of Fluids*, Vol. 14, No. 2, February 2002, pp. 851-861.
5. Brown, G., Roshko, A., "On density effects and large structure in turbulent mixing layers"; *J. Fluid Mech.*, Vol. 64 part 4, 1974, pp. 775-816
6. Papamoschou D., Roshko, A., "The compressible turbulent shear layer: an experimental study," *J. Fluid Mech.* Vol. 197, No. 453 1988
7. Dimotakis, P. E., "Two-Dimensional Shear Layer Entrainment", *AIAA Journal*, Vol. 24, No. 11, Nov. 1986, pp. 1791-1796
8. Leyva, I. A., Rodriguez, J. I., Chehrودي, B., Talley, D., "Preliminary Results on Coaxial Jets Spread Angles and the Effects of Variable Phase Transverse Acoustic Fields", *AIAA-2008-0950*
9. Rodriguez, J. I., Leyva, I. A., Chehrودي, B., Talley, D., "Effects of a Variable-Phase Transverse Acoustic Field on a Coaxial Injector at Subcritical and Near-Critical Conditions", *ILASS Americas*, 21st Annual Conference on Liquid Atomization and Spray Systems, Orlando, Florida, May 18-21 2008.
10. Leyva, I. A., Chehrودي, B., Talley, D., "Dark-core analysis of Coaxial Injectors at Sub-, Near-, and Supercritical Conditions in a Transverse Acoustic Field", *AIAA-2007-5456*
11. Leyva, I. A., Chehrودي, B., Talley, D., "Dark-core analysis of Coaxial Injectors at Sub-, Near-, and Supercritical Conditions in a Transverse Acoustic Field", *54<sup>th</sup> JANNAF Meeting*, Denver, CO, May 14-18, 2007.
12. REFPROP, Reference Fluid Thermodynamic and Transport Properties, Software Package, Ver. 7.0, NIST, U.S. Department of Commerce, Gaithersburg, MD, 2002.
13. Thermophysical Properties of Fluid Systems (<http://webbook.nist.gov/chemistry/fluid>), NIST, U.S. Department of Commerce, Gaithersburg, MD, 2005
14. Otsu, N., *IEEE transactions on Systems, Man, and Cybernetics* 1:62-66 (1979).
15. Davis, D.W., Chehrودي B., "Measurements in an acoustically driven coaxial jet under sub-, near-, and supercritical conditions", *JPP*, Vol. 23, No. 2, March-April 2007
16. Favre-Marinet, M., Camano Schettini, E.B., "The density field of coaxial jets with large velocity ratio and large density differences", *Int. J. of Heat and Mass Transfer*, 44 (2001) pp. 1913-1924
17. Liu T., Zong, N., Yang, V., "Dynamics of Shear-Coaxial Cryogenic Nitrogen Jets with Acoustic Excitation under Supercritical Conditions", *AIAA* 2006-759.
18. Leyva, I. A., Rodriguez, J. I., Chehrودي, B., Talley, D., "Effect of phase angle on coaxial jet behavior spanning sub- to supercritical pressures", *ILASS Europe*, 2008

## APPENDIX

### A. Case Details for the One-Phase Subcritical Coaxial Jet Spreading Angle Study

	T <sub>chamber</sub> (K)	ρ <sub>chamber</sub> (kg/m <sup>3</sup> )	P <sub>chamber</sub> (MPa)	T <sub>outer</sub> (K)	$\dot{m}$ <sub>outer</sub> (mg/s)	ρ <sub>outer</sub> (kg/m <sup>3</sup> )	u <sub>outer</sub> (m/s)	T <sub>inner</sub> (K)	$\dot{m}$ <sub>inner</sub> (mg/s)	ρ <sub>inner</sub> (kg/m <sup>3</sup> )	u <sub>inner</sub> (m/s)	VR	MR	tan α <sub>1</sub> + tan α <sub>4</sub>
<b>SUB</b>														
angle1	276	18.0	1.47	250	304	20	5.8	145	281	38	36	0.16	0.013	-0.12
angle2	276	18.8	1.53	254	506	21	9.2	145	281	40	35	0.27	0.037	0.08
angle3	276	18.2	1.48	254	1000	20	19	150	281	36	39	0.50	0.14	0.15
angle4	270	19.2	1.53	245	2000	21	36	155	282	36	39	0.94	0.52	0.17
angle5	270	18.8	1.50	246	3010	21	55	148	282	38	37	1.5	1.2	0.17
angle6	261	20.1	1.54	242	4500	22	78	190	281	28	50	1.6	2.0	0.26

### B. Case Details for the Subcritical to Supercritical Coaxial Jet Dark Core Length Study

	T <sub>chamber</sub> (K)	ρ <sub>chamber</sub> (kg/m <sup>3</sup> )	P <sub>chamber</sub> (MPa)	T <sub>outer</sub> (K)	$\dot{m}$ <sub>outer</sub> (mg/s)	ρ <sub>outer</sub> (kg/m <sup>3</sup> )	u <sub>outer</sub> (m/s)	T <sub>inner</sub> (K)	$\dot{m}$ <sub>inner</sub> (mg/s)	ρ <sub>inner</sub> (kg/m <sup>3</sup> )	u <sub>inner</sub> (m/s)	Freq. (kHz)	P' <sub>RMS</sub> (kPa)	VR	MR
<b>SUB</b>															
sub1	233	22.0	1.50	191	310	22.0	4.30	109	279	630	2.2	2.98	21.5	2.0	0.17
sub2	231	22.2	1.50	183	790	28.8	11.0	109	283	630	2.2	3.06	20.1	4.8	1.0
sub3	226	21.9	1.45	183	1230	27.8	16.9	109	284	630	2.2	3.06	17.8	7.6	2.6
sub4	226	22.9	1.51	185	1560	28.7	20.9	109	279	630	2.2	2.96	15.7	9.5	4.2
sub5	210	24.9	1.50	182	2400	29.3	31.3	109	279	630	2.2	3.01	16.9	14	9.6
sub6	216	24.1	1.50	191	3640	27.7	50.3	109	279	630	2.2	3.02	16.3	23	23
<b>NEAR</b>															
near1	223	56.6	3.58	180	1060	75.4	5.38	123	290	520	2.8	3.08	9.04	2.0	0.55
near2	207	62.0	3.57	152	1570	101	5.95	117	289	590	2.4	3.04	10.8	2.5	1.0
near3	228	55.1	3.58	185	1590	72.4	8.40	126	293	440	3.3	3.00	11.8	2.6	1.1
near4	223	56.1	3.55	184	2170	72.3	11.5	127	294	360	4.0	3.01	11.4	2.8	1.6
near5	230	54.2	3.56	199	2120	65.1	12.5	126	292	440	3.3	3.03	12.1	3.8	2.1
near6	229	54.5	3.56	183	2690	73.1	14.1	126	292	420	3.4	3.05	11.1	4.1	2.9
near7	219	57.6	3.56	194	3080	67.4	17.5	125	289	480	3.0	3.06	11.8	5.9	4.9
near8	213	59.6	3.56	192	6460	68.3	36.2	128	295	220	6.6	2.93	9.73	5.5	9.3
<b>SUPER</b>															
super1	231	76.1	4.96	198	292	93.9	1.19	136	291	300	4.8	3.05	8.01	0.25	0.019
super2	231	76.1	4.96	193	997	97.7	3.90	130	292	460	3.1	3.01	10.2	1.2	0.33
super3	221	80.4	4.95	180	2050	109	7.19	128	291	490	2.9	3.01	10.7	2.5	1.3
super4	222	80.1	4.96	182	3110	107	11.1	134	288	360	3.9	3.05	10.1	2.8	2.4
super5	222	80.3	4.97	191	2820	99.5	10.8	131	293	440	3.3	3.09	12.5	3.3	2.5
super6	211	85.8	4.96	187	5820	103	21.6	132	286	410	3.4	3.05	10.7	6.3	9.9